Intravascular delivery of an ultraflexible neural electrode array for recordings of cortical spiking activity

Xingzhao Wang[1], Shun Wu[1], Hantao Yang[2,3], Yu Bao[1,4], Zhi Li[5], Changchun Gan[1], Yuanyuan Deng[6], Junyan Cao[7], Xue Li[1], Yun Wang[3,5], Chi Ren [1] ✉, Zhigang Yang [3] ✉ & Zhengtuo Zhao [1,4] ✉

Although intracranial neural electrodes have significantly contributed to both fundamental research and clinical treatment of neurological diseases, their implantation requires invasive surgery to open craniotomies, which can introduce brain damage and disrupt normal brain functions. Recent emergence of endovascular neural devices offers minimally invasive approaches for neural recording and stimulation. However, existing endovascular neural devices are unable to resolve single-unit activity in large animal models or human patients, impeding a broader application as neural interfaces in clinical practice. Here, we present the ultraflexible implantable neural electrode as an intravascular device (uFINE-I) for recording brain activity at single-unit resolution. We successfully implanted uFINE-Is into the sheep occipital lobe by penetrating through the confluence of sinuses and recorded both local field potentials (LFPs) and multi-channel single-unit spiking activity under spontaneous and visually evoked conditions. Imaging and histological analysis revealed minimal tissue damage and immune response. The uFINE-I provides a practical solution for achieving high-resolution neural recording with minimal invasiveness and can be readily transferred to clinical settings for future neural interface applications such as brain-machine interfaces (BMIs) and the treatment of neurological diseases.

Neural electrodes are the key to establishing high-performance brain-machine interfaces (BMIs). The development of different types of electrodes, especially the intracranial electrodes, has significantly contributed to both fundamental neuroscience research and clinical applications[1,2]. For example, Utah arrays have been extensively used for movement restoration in BMIs, enabling dexterous control of external devices based on the neural spiking activity[3–5]. SEEG (stereo-electroencephalography) and DBS (deep brain stimulation) electrodes have become essential tools for monitoring and modulating brain activity to treat neurological diseases, such as epilepsy and Parkinson's disease[6–9]. The extraordinary sampling power of Neuropixels probes has revolutionized the way we study and understand the brain function[10,11]. However, these electrodes are made of rigid materials (e.g., metal or silicon based), suffering from signal degradation or unstable modulation effects due to accumulated glial scars in the surrounding tissues over long-term implantation[12,13]. In contrast, ultraflexible microelectrodes have demonstrated excellent biocompatibility, forming seamless neuron-electrode interfaces for stable

[1]Institute of Neuroscience, Center for Excellence in Brain Science and Intelligence Technology, Chinese Academy of Sciences, Shanghai, China. [2]Shanghai Geriatric Medical Center, Shanghai, China. [3]Zhongshan Hospital, Shanghai, China. [4]University of Chinese Academy of Sciences, Beijing, China. [5]Fudan University, Shanghai, China. [6]ShanghaiTech University, Shanghai, China. [7]University of Shanghai for Science and Technology, Shanghai, China. ✉e-mail: renc@ion.ac.cn; yang.zhigang1@zs-hospital.sh.cn; zhaozt@ion.ac.cn

long-term recording and modulation of brain activity[14–17]. Nevertheless, these intracranial electrodes require open craniotomy for direct implantation into the brain, exacerbating the risk of inflammatory tissue responses and thus impairing the brain function[18–20]. Hence, there is an urgent need to explore minimally invasive approaches to address these challenges.

Interventional approaches have become the preferred choice in the treatment of many neurological diseases due to the avoidance of craniotomy, favorable outcomes, and shorter hospital stays[21,22]. The emergence of versatile interventional tools in recent decades has created a fertile ground for development of neurointerventional devices[23–25]. Notable examples include the Detachable Coil System (Medtronic), designed for intricate peripheral embolization[26], and the Reperfusion Catheter (Penumbra), employed for the revascularization in acute ischemic stroke[27,28]. Therefore, the interventional strategy is a promising candidate to minimize the invasiveness of electrode implantation. Several pilot studies have explored the feasibility of deploying interventional tools for electrode delivery in both animal models as well as human patients. Stentrode, an endovascular macroelectrode derived from a self-expanding nitinol stent, has achieved vascular electrocorticography (ECoG) recording and stimulation in sheep superior sagittal sinus (SSS) and progressed to clinical trials for motor neuroprostheses in human patients with severe paralysis[29,30]. Patients could use electrocorticography signals to control multiple mouse-click actions and achieve cursor navigation with the assistance of an eye-tracker. On the other hand, a mesh-like ultraflexible microelectrode has recently been introduced as an endovascular probe, and successfully recorded single-unit spikes from sub-100 μm-scale blood vessels in rat brains, offering a minimally invasive option to record spiking activity[31]. However, only a few single units were recorded endovascularly from the rat olfactory bulb, questioning its generalizability to other brain regions and larger animal models, and ultimately to human clinical applications. Nevertheless, these pioneering studies demonstrate the safety of intravascular implantation of neural electrodes, but meanwhile, raise the need for more effective intravascular solutions.

Based on the existing studies, we believe that placing microelectrodes through blood vessels into the brain after endovascular delivery is the key step to achieving minimally invasive, high-resolution, and stable neural interfaces that can actually be translated to clinical applications. The ultraflexibility and micron-scale dimensions make the ultraflexible microelectrode ideal for this procedure for the following two reasons. First, it is well suited for navigating tortuous blood vessels, reaching various brain regions via small distal branches. Second, it also minimizes the risk of bleeding during penetration, facilitating the sealing between the ultraflexible microelectrode and vessels. The feasibility of penetrating through the intracranial veins has been convincingly demonstrated by the eShunt System (CereVasc), which addresses the communicating hydrocephalus by creating a pathway to shunt the cerebrospinal fluid into the venous system[32,33].

Here we present an ultraflexible implantable neural electrode (uFINE-I) capable of recording single-unit spiking activity in the sheep brain via intravascular delivery. A corresponding intravascular implantation system was meticulously designed to fulfill the requirements for effective delivery and penetration through brain blood vessels, which is typically challenging to conventional devices. Using this strategy, we managed to implant the uFINE-I in the sheep occipital lobe and recorded both local field potentials (LFPs) and multi-channel single-unit spikes under spontaneous and visually evoked conditions. Postoperative imaging and histological analysis revealed minimal tissue damage and little immune response. Implantation of uFINE-Is in multiple brain regions was demonstrated using a silicone model of the human intracranial venous system. This platform offers a minimally invasive solution that will enable high-resolution neural recording and stimulation for a variety of scenarios in both fundamental neuroscience research and clinical applications.

Design of the uFINE-I and implantation device

To record single-unit spiking activity via intravascular strategy, the uFINE-I needs to be implanted into the brain tissue by penetrating through the blood vessel wall. To minimize the risk of bleeding during penetration, we specifically focused on the feasibility of navigating and penetrating through cerebral veins as venous blood pressure is lower than intracranial pressure. We identified the confluence of sinuses as the candidate to validate our intravascular implantation system because of its proximity to the visual cortex. Neural activity in the visual cortex, especially visually evoked responses, provides an intuitive assessment of the recording capability of neural electrodes[15,16].

To validate our intravascular strategy for uFINE-I implantation, we selected sheep as our animal model as its intracranial venous structure is comparable to that of humans[34,35], which will facilitate easy transfer to future clinical applications (Supplementary Table 1). We first characterized the anatomy of the sheep intracranial venous system via advanced digital subtraction angiography (DSA) technology to determine the delivery path and size limits of intravascular devices (Fig. 1a and Supplementary Fig. 1). The confluence of sinuses intersects two laterally oriented TrS branches that converge towards the apex and extend distally along the DSS. Similar to that in humans, the sheep confluence of sinuses is also close to the occipital lobe that participates in vision processing[36], creating a suitable site for implanting electrodes into the brain tissue via penetrating through the vessel wall (Fig. 1b).

Based on the anatomical measurements of sheep intracranial veins (Fig. 1a and Supplementary Fig. 1), we designed a delivery path and meticulously selected mature, commercially available catheters and guidewires to assemble a unique implantation system for uFINE-I (Fig. 1c-f and Supplementary Table 2). The pathway extended from the internal jugular vein to the sigmoid sinus (SiS, with a diameter of ~5.79 mm) and then continued to the transverse sinus (TrS, with a diameter of ~2.30 mm) (Supplementary Fig. 1). A balloon catheter system was included as an add-on, allowing fine-tuning the device position relative to the cortex before penetration, if necessary (Fig. 1b). The piercing device was composed of a proximal handle, a custom-designed microcatheter for smooth delivery, a microneedle for vessel wall penetration, and a guiding microwire to further insert the uFINE-I to the desired location (Fig. 1c–e). The microcatheter, ~400 mm long with an outer diameter of 1.7 F (0.57 mm), is the most popular neurointerventional microcatheter commercially available that can fit into the sheep intracranial veins and be directly transferred to future clinical trials. The puncture microneedle and guiding microwire were placed within this microcatheter, which could be progressively protruded and retracted through manipulation of the proximal handle. The uFINE-I was hitched to the guiding microwire through a 35 μm ring-shaped structure at the probe tip, and the rest of the uFINE-I shank was housed in the space between the microcatheter and microneedle (Fig. 1e,f). This ingenious mechanism facilitates the insertion of electrodes guided by the microwire into the brain tissue, ensuring a minimally invasive implantation procedure.

To accommodate the long delivery path (330–350 mm) from the jugular vein to the confluence of sinuses and the tiny space (0.05–0.06 mm) between the microcatheter and puncture microneedle (Fig. 1f), we exploited state-of-the-art micro/nano fabrication techniques, and managed to fabricate the uFINE-I with a total length of 50 cm, a thickness of 5 μm, and an average width of 120 μm (Fig. 1g-i and Supplementary Fig. 2). Polyimide (PI) was used as the base material as its high tensile strength ensured the integrity of uFINE-I during navigation and penetration[16]. Each uFINE-I accommodated a linear array of 30 electrode sites distributed along the tip, with an electrode site diameter of 30 μm and inter-electrode center distance of 40 μm.
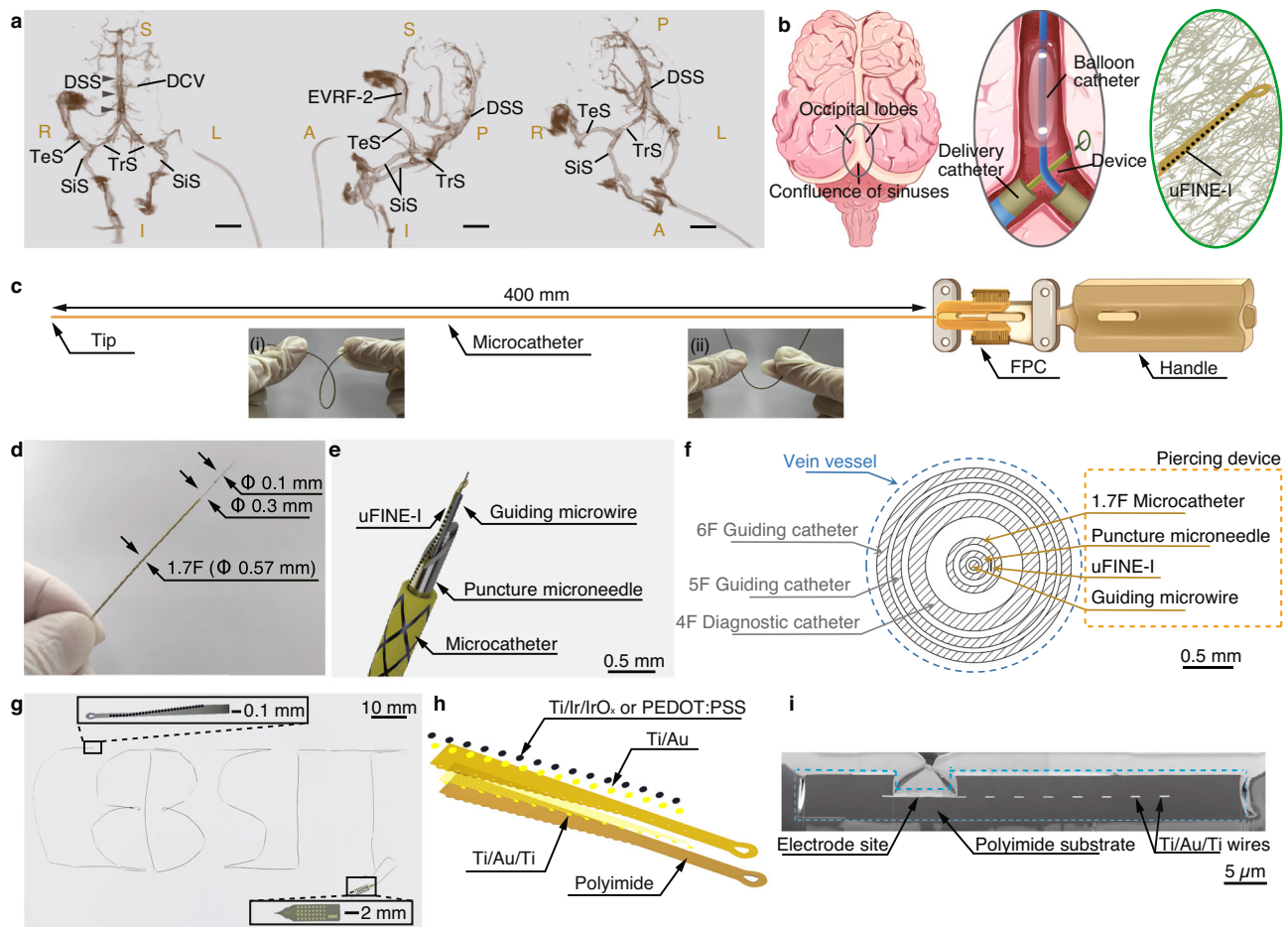
Fig. 1 | An overview of the uFINE-I and intravascular implantation system.
a DSA images of the sheep intracranial venous system, showing the confluence of sinuses and its connecting venous branches from different angles. These structures include the dorsal cerebral vein (DCV), dorsal sagittal sinus (DSS), sigmoid sinus (SiS), temporal sinus (TeS), transverse sinus (TrS), and the second emissary vein of the retroarticular foramen (EVRF-2). A: anterior, P: posterior, R: right, L: left, S: superior, I: inferior. Scale bars, 10 mm. **b** Schematic diagram showing the dorsal view of the relative position between the sheep venous system and the brain tissue. The left ellipse represents the target zone around the confluence of sinuses for the implantation system, and the right ellipse shows the uFINE-I probe in the brain tissue after penetration, surrounded by neurons. **c** Schematic diagram showing the piercing device. Insets show its twisting (i) and bending (ii) properties. The FPC (flexible printed circuit) board connected to the uFINE-I was held between the handle and the microcatheter. **d** Picture of the piercing device tip. **e** Schematic diagram showing individual layers of the piercing device tip. **f** Cross-sectional view of the intravascular implantation system, showing the assembly of the piercing device located in the lumen of catheters. **g** Picture of a 50-cm long uFINE-I probe shaped in the form of uppercase letters "CEBSIT", showing the length and flexibility of the uFINE-probe. Magnified views show the tip accommodating electrode sites (top) and the connecting pad (bottom). **h** Exploded view schematic diagram showing the probe tip. **i** The focus ion beam (FIB) image showing the cross-sectional structure of uFINE-I, marked by the blued dashed rectangle.

These electrodes covered a total range of ~1.2 mm, allowing for an extended spatial coverage of neural recording. To achieve a better quality of single-unit recording, the electrode was coated with IrO_x (iridium oxide) or PEDOT:PSS (poly(3,4-ethylenedioxythiophene)-poly(styrenesulfonate)) to reduce the impedance to ~100 kΩ.

Fabricating the macro-scaled uFINE-Is (50 cm long, Fig. 1c, e) with micro-scale resolution (1.5 µm line width and spacing, Fig. 1i) presented significantly more challenges to obtaining high fabrication yield compared to typical MEMS-based devices at the scale of a few millimeters to centimeters. We deployed the following technical modifications to improve yield. First, a strictly high cleanliness level was enforced during fabrication. Based on our experience, at the same cleanliness level, the electrode failure rate per probe due to particle contamination quickly increases with the probe length. To minimize the electrode failure caused by particle contamination, most fabrication steps required a higher cleanroom standard, improved from Class 1000 (ISO 6) for typical MEMS-based neural electrodes to Class 100 (ISO 5). Furthermore, the wafer was cleaned by sonication and gently wiping with cleanroom wipers in the solvent. A microscopic examination of the entire structure was performed for quality check before

proceeding to the next step. Second, the sacrificial layer was omitted to prevent electrode failure resulting from prolonged exposure to etchants during the extended-release process of longer probes. Instead, the uFINE-Is were directly peeled from the silicon substrate. After technical improvements, the average electrode yield per uFINE-I probe increased from 33% to 65% (best: 50% to 90%). Additionally, to fit the long and tortuous intravascular pathway, a delicate balance between the strength and flexibility of interventional probes was achieved through meticulous adjustments of structural design and fabrication processes (see "Methods" for details).

Implantation of uFINE-I via intravascular delivery

The structure of sheep intracranial veins also brought extra challenges to device delivery than that in the human venous system. First, the venous path to the confluence of sinuses is highly branching and tortuous. Particularly, the stenotic segments in the TrS and EVRF-1 as well as the EVRF-1/EVRF-2 bifurcation exacerbate the navigating difficulty (Fig. 2a). Second, this path first passes through the soft neck tissue and then the hard skull via the emissary foramen, experiencing a sudden change in mechanical properties of the surrounding tissues. Third, the
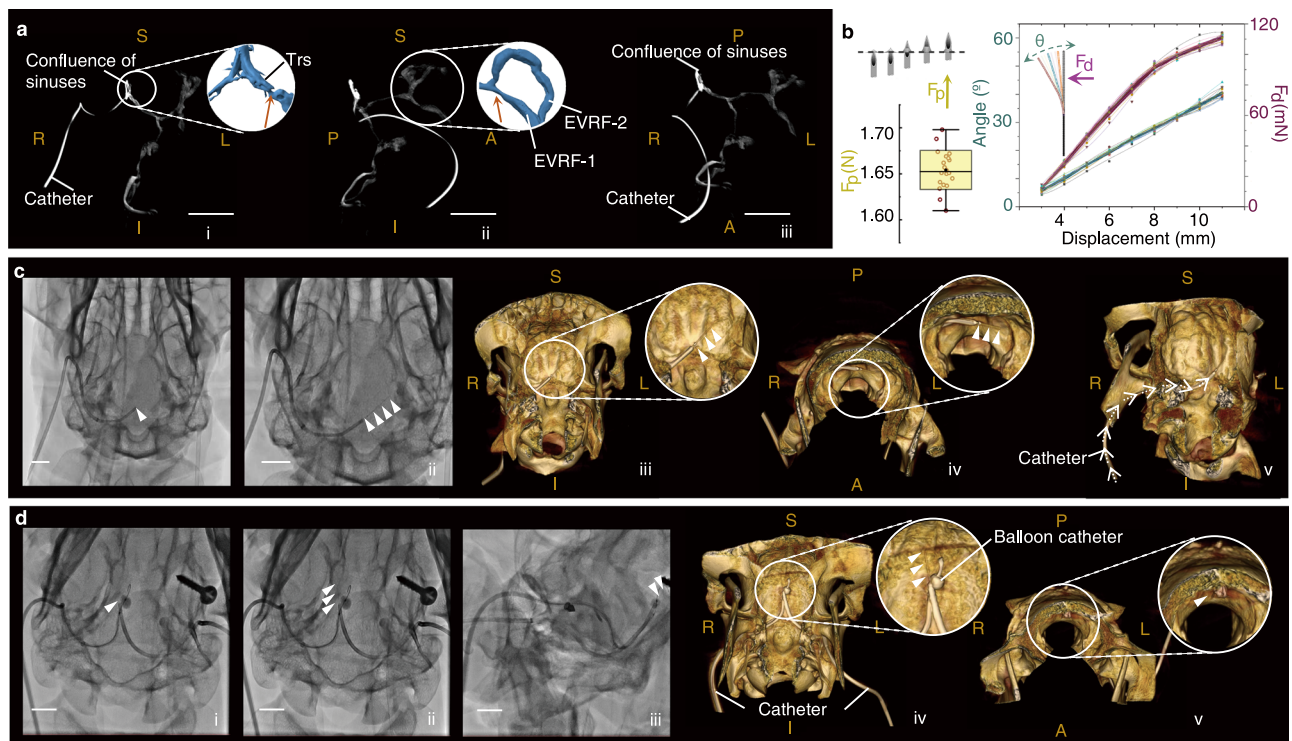
Fig. 2 | Intravascular device implantation. a Neck and intracranial angiography with maximum intensity projection (MIP) technique showing the anterior (i), lateral (ii), and oblique (iii) views of the venous path from the jugular vein to the confluence of sinuses, embedded in a highly intricate and tortuous venous network for device navigation. Red arrows indicate the stenotic segments. A: anterior, P: posterior, R: right, L: left, S: superior, I: Inferior. Scale bars, 10 mm. **b** Left, puncture force (F_p) measurement of the tip of microneedle. Boxed plots: the 25th, 50th (median), and 75th percentiles of the data ($n = 20$) are indicated. The whiskers represent minimum and maximum values. Right, bending properties of a 20-mm long microneedle, showing the bending angle and deflection force at different tip displacements. Error bars, SD. **c** Penetration at the confluence of sinuses without the balloon catheter system. DSA images showing the location of the microneedle before (i) and after (ii) penetration. The penetration direction was confirmed using DSA 3D reconstruction (iii-v). Arrowheads mark the location of the microneedle tip. Arrows in (v) indicate the trajectory of the piercing device. **d** Penetration assisted by a balloon catheter system. DSA images showing the location of the microneedle before (i) and after (ii, iii) penetration. The penetration direction was confirmed using DSA 3D reconstruction (iv, v). Arrowheads mark the location of the microneedle tip. Scale bars in (**c**) and (**d**), 10 mm.

sheep intracranial venous system exhibits strong anatomical idiosyncrasies, and even the left and right sides within the same sheep are distinct. All these factors collectively require a delicate balance between the flexibility and rigidity of the intravascular piercing device; it has to be flexibly adjusted to accommodate the complicated venous paths, but meanwhile rigid enough to transmit the puncture force for penetration.

In line with these requirements, we meticulously designed a nickel-titanium tube as the skeleton of the piercing device. This nickel-titanium tube featured a precision-cut tip, serving as the puncture microneedle. The average puncture force (F_p) was -1.65 N, measured rigorously in accordance with international ISO standards (Fig. 2b, left). Meanwhile, the nickel-titanium tube exhibited sufficient flexibility (Fig. 2b, right). A 55° reflection angle (θ) of the 20 mm tip required only 120 mN deflection force (F_d), allowing navigating all tortuous structures safely along the venous path.

For intravascular implantation of uFINE-I in sheep (Supplementary Fig. 3), we experienced significant individual variations in venous structures when determining the pathway at the following two points: the choice between the left and right sigmoid sinus (SiS) and transverse sinus (TrS), and between the EVRF-1 and EVRF-2 branches, requiring careful examination of the preoperative DSA images and sometimes exploratory navigation to select a feasible venous pathway. We first established an implantation pathway from the jugular vein to the confluence of sinuses using a set of commercially available catheters, each varying in size (4, 5, and 6 F profile, Supplementary

Fig. 1, Supplementary Table 2, Supplementary Movies 1 and 2). Then the piercing device carried the uFINE-I navigating through the constructed pathway until it reached the confluence of sinuses (Supplementary Movie 1). To ensure a successful penetration into the brain, the position of device tip was meticulously examined using DSA both before and after penetration (Fig. 2c, and Supplementary Fig. 4a). Before penetration, we carefully adjusted the tip position towards the direction more perpendicular to the cortex. It is noteworthy that the direction of penetration occurred at an angle deviating from the parallel alignment with the DSS (Fig. 2c, iii). Additionally, the microneedle also exhibited a subtle inclination relative to the inner surface of the skull, suggesting that the microneedle pointed to the brain (Fig. 2c, iv and Supplementary Fig. 4a, iii). Due to the individual anatomical variations of the sheep intracranial venous system, in some circumstances, we employed a balloon catheter system under the guidance of DSA to further constrain the piercing device to the desired angle (Fig. 2d and Supplementary Fig. 4b). After penetration, the uFINE-I was further protruded into the brain tissue by 3–7 mm at a speed of 0.1 mm/s via pushing the guiding microwire through manual manipulation of the proximal handle. The estimated final insertion point of uFINE-I was 1–3 mm posterior, 2–5 mm lateral, and 4–8 mm deep relative to the middle of the confluence of sinuses. Throughout the entire surgery, the catheter delivery process took -1 h, primarily due to navigation in the intricate sheep venous system. Following the successful arrival at the target location, the evaluation of the device position took -0.5 h. Device penetration only took 2–5 min.
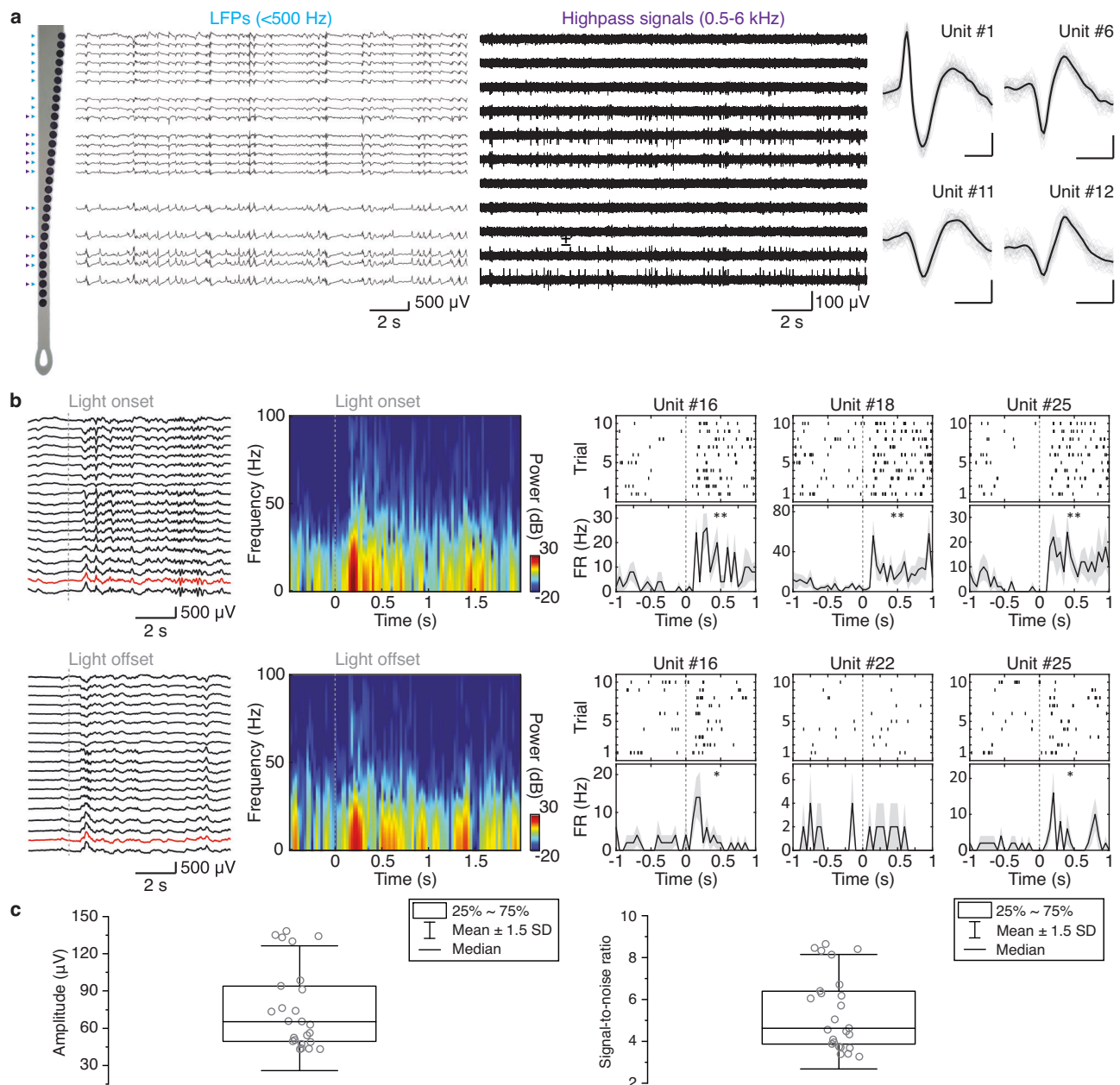
Fig. 3 | Electrophysiological recording via uFINE-I in the sheep occipital lobe under light anesthesia. a An example of spontaneous activity recorded by distributed uFINE-I channels, showing the LFPs (<500 Hz, left), spiking activity (0.5–6 kHz, middle), and waveforms of individual single units isolated by spike sorting (right). A short period of recording was presented for a better visualization of the spiking activity. LFPs were only shown for channels with impedance < 4 MΩ, corresponding to electrode sites pointed by blue arrows in the schematic diagram of uFINE-I. Example channels showing highpass-filtered spiking activity correspond to electrode sites pointed by purple arrows. Each waveform is represented by an average of 50 traces. Vertical scale bars, 25 μV, horizontal scale bars, 0.5 ms. **b** Visually evoked neural responses to the light onset (top) and offset (bottom).

LFPs exhibited increased fluctuations immediately after the light onset/offset (left), with a power increase in the beta and gamma bands (12–30 and 30–80 Hz, middle, corresponding to the channel in red on the left). Raster plots and firing rates for example single units responsive or nonresponsive to the light onset/offset (right). Shaded areas indicate SEM. $n = 10$ trials for each unit, two-side Wilcoxon signed rank test, * $P < 0.05$, ** $P < 0.01$. FR: firing rate. **c** Peak-to-trough spike amplitude (left) and signal-to-noise ratio (right) of single units ($n = 25$) recorded under spontaneous and visual stimulation conditions. Boxed plots: the 25th, 50th (median), and 75th percentiles of the data are indicated. The whiskers represent mean ± 1.5 SD.

Electrophysiological recording by uFINE-I

To evaluate the recording capability of uFINE-Is, especially the possibility of resolving single-unit spiking activity, we performed electrophysiological recording immediately after inserting the uFINE-I into the occipital lobe of sheep under light anesthesia (Fig. 3 and Supplementary Fig. 6). An example recording showed spontaneous LFP activity (< 500 Hz) along the distributed recording channels (Fig. 3a, left, and Supplementary Fig. 6a). Importantly, we observed spiking

activity from multiple channels at different locations (0.5–6 kHz, Fig. 3a, middle, and Supplementary Fig. 6a). Based on the spike waveform and autocorrelogram (Supplementary Fig. 5), we successfully sorted spikes to individual single units, which showed high peak-to-trough amplitudes (Fig. 3a, right). To further examine whether the uFINE-I could reveal behaviorally relevant brain activity, we flickered a flashing light in front of the contralateral eye as visual stimuli during electrophysiological recording in the occipital lobe. LFP signals
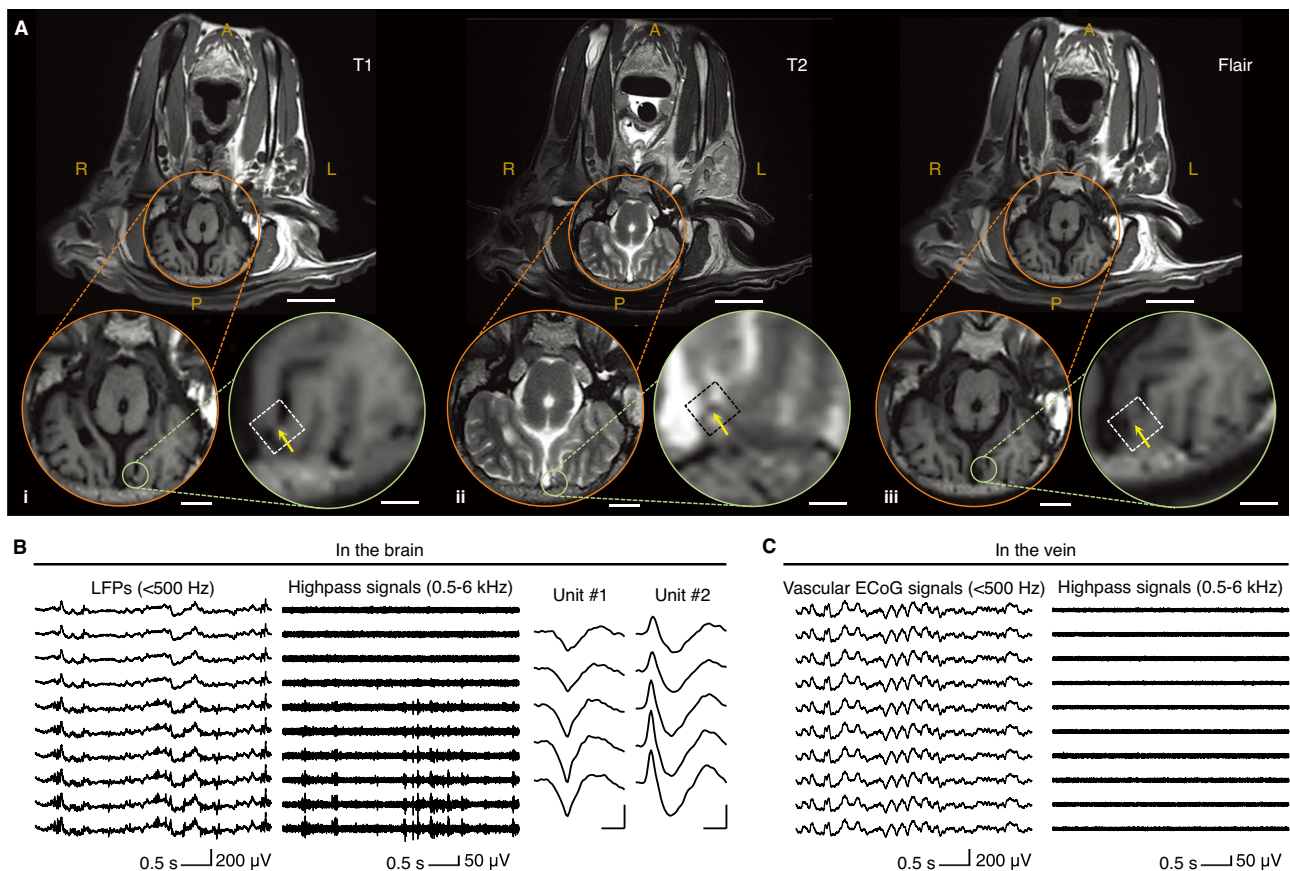
Fig. 4 | Electrode-only retention of uFINE-I in the sheep brain. A Horizontal views of three distinct 1.5-T MRI sequences (T1 (i), T2 (ii), and Flair (iii)) showing the uFINE-I retained in the brain. Magnified views in circles correspond to the area circled by the same color in zoom-out images. The uFINE-I location was marked by dashed rectangles and further pointed by yellow arrows. A: anterior, P: posterior, R: right, L: left. Scale bars, 2 cm, 0.5 cm, and 0.1 cm as magnification increases. **B** An example of activity recorded by uFINE-I independently retained in the brain, showing the LFPs (< 500 Hz, left), spiking activity (0.5–6 kHz, middle), and waveform spread of example single units (right). Vertical scale bars, 25 µV, horizontal scale bars, 0.5 ms. **C** An example of activity recorded by uFINE-I retracted into the vein lumen. Note that no spiking activity was detected in highpass-filtered signals.

exhibited strong modulation time-locked to the light onset and offset (Fig. 3b, left, and Supplementary Fig. 6b), especially around the beta (12−30 Hz) and gamma (30−80 Hz) bands (Fig. 3b, middle), consistent with previous reports[16]. At the sing-cell level, we also identified single units that were responsive or nonresponsive to the light onset and offset[37,38] (Fig. 3b, right). In total, 36% of single units showed significant responses to light onset or offset. These results validated the recording capability of uFINE-Is to reveal behaviorally relevant information in neural activity. In total, we recorded 25 single units from this sheep. The average peak-to-trough spike amplitude and signal-to-noise ratio were 76.08 µV and 5.42, respectively (Fig. 3c). In conclusion, these results demonstrate that the uFINE-I and corresponding intravascular implantation strategy are capable of recording single-unit spiking activity in the brain at scale.

Electrode-only retention of uFINE-I in the brain
Although the microwire-guided uFINE-I was capable of single-unit recording, only retaining the uFINE-I in the brain is fundamental to fully exploiting the advantages of ultraflexible electrodes in chronic implantation. To validate that the uFINE-I could be retained in the brain after retracting the guiding microwire, we first confirmed its location under magnetic resonance imaging (MRI). As the uFINE-I was too tiny to be detected under MRI, we engineered a specialized dummy uFINE-I, which had an additional nickel metal layer for MRI detection. During implantation, we used a microwire to guide the uFINE-I to the desired location within the brain. Subsequently, upon reaching the desired

position, the microwire was retracted from the brain, leaving only the uFINE-I in the brain tissue. After microwire retraction, the dummy uFINE-I was detected in the occipital lobe from all three distinct 1.5-T MRI sequences (T1, T2, and Flair, Fig. 4A), evident from the disruption of the uniform brain tissue by the metal artifacts from the dummy uFINE-I, validating the independent retention of uFINE-I in the brain. A post-mortem examination of the same sheep brain further confirmed that the uFINE-I was located in the brain tissue in proximity to the confluence of sinuses (Supplementary Fig. 7). In addition, we performed an in vitro test in 1% agarose gel, showing a neglectable displacement of the uFINE-I tip during guiding microwire retraction (Supplementary Movie 3).

To evaluate the recording capability of the independently retained uFINE-I, we compared the signals recorded in two different situations: the uFINE-I retained in the brain tissue and the uFINE-I retracted into the vein lumen (Figs. 4B, C). The independently retained uFINE-I was still capable of recording single-unit spiking activity in the brain (Fig. 4B). However, when the uFINE-I was retracted into the vein lumen, no spiking activity was detected (Fig. 4C), emphasizing the necessity of implanting the electrode into the brain for single-unit recording. These results demonstrate that the independently retained uFINE-I maintains the ability to resolve single-unit spiking activity.

Safety assessment of uFINE-I implantation
To assess the safety of our intravascular implantation strategy, we conducted a comprehensive study involving three groups of animals,
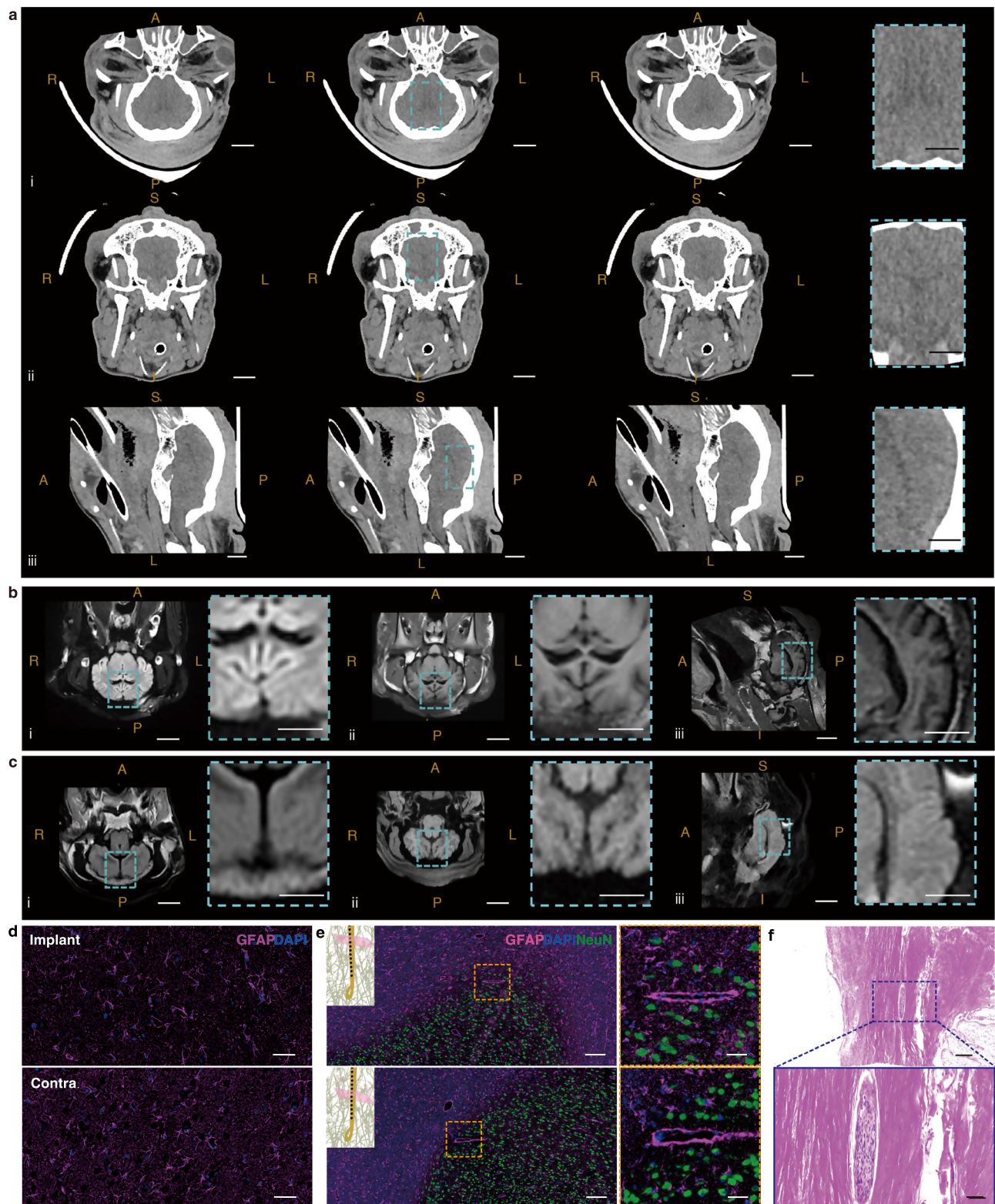
examining them immediately after the surgery and at 7 and 30 days postoperatively to identify any potential risks (Supplementary Table 1). Given the possibility of microbleeding during device penetration, we conducted computed tomography (CT) scans on the operated animals immediately after the surgery. Figure 5a shows postoperative CT images around the penetration site from three axial planes of a sheep brain. In the magnified view of the coronal plane (Fig. 5a, iv), we observed no discernible signs of bleeding within the brain tissue. No

microbleeding was detected in three animals with immediate post-operative CT scans (Fig. 5a and Supplementary Fig. 8). Consistently, in a post-mortem examination performed immediately after the surgery, we noticed that the device penetration only created a minuscule hole in the brain, causing minimal bleeding in the surrounding tissues (Supplementary Fig. 7). In addition, it is noteworthy that the sheep exhibited the ability to stand upright independently on the second day following the surgical procedure (Supplementary Movie 4). These

Fig. 5 | Safety assessment of intravascular implantation and viability in human clinical settings. a Postoperative CT images around the estimated penetration site from an example sheep brain, showing the intact brain tissue from three axial planes. The magnified view corresponds to the region in the blue dashed rectangles. Three successive slices spanning 1 mm were shown for each plane. A: anterior, P: posterior, R: right, L: left, S: superior, I: Inferior. Scale bars, 2 cm and 1 cm in the magnified view. **b** and **c**, MRI scans (1.5-T, Flair (i), T1 (horizontal and sagittal views, ii and iii)) revealing brain tissue integrity at 7 (**b**) and 30 (**c**) days post the surgery. The magnified views correspond to the region in the blue dashed rectangles in (ii). Scale bars, 2 cm and 1 cm in the magnified view. **d** Fluorescent images of tissue sections at 30 days after acute uFINE-I implantation, showing no

detectable tissue damage caused by implantation. GFAP marks astrocyte activation, a sign of immune response, and DAPI stains nuclei. Scale bar, 50 μm. **e** Fluorescent images showing two tissue sections along the implantation trajectory (indicated by the pink plane in the inset) after 30-day chronic uFINE-I implantation. Magnified views showing the electrode footprints corresponding to the region in the orange dashed rectangles in the zoomed-out images. NeuN marks mature neurons. Scale bars, 200 μm and 50 μm. **f** Hematoxylin and Eosin (HE) staining of penetration scar, showing healing with spindle cell hyperplasia 30 days after penetration. The magnified view corresponds to the region in the blue dashed rectangle. Scale bars, 200 μm and 50 μm. **d**–**f** The experiment was repeated three times, showing similar results.

results provide conclusive evidence that the penetration process did not cause acute clinical hemorrhagic damage to the brain.

To confirm whether there were any long-lasting effects of the intravascular implantation procedure, we scanned the brain again by MRI at 7 and 30 days after the surgery (Figs. 5b, c). Brain tissues near the implantation site exhibited high integrity and no discontinuous dark areas indicating tissue damage were observed. A histology study was also performed on the brain and main internal organs collected 30 days after the acute implantation. Neither lesions nor elevated immune response was detected near the implantation site (Supplementary Fig. 9 and Fig. 5d). Furthermore, none of the main internal organs showed discernible signs of abnormality (Supplementary Fig. 8). These results demonstrate minimal invasiveness of our intravascular implantation strategy.

To further examine the long-term biocompatibility and safety of uFINE-Is, we left the uFINE-I probe in the sheep occipital lobe chronically for 30 days in another sheep. Consistent with previous reports[14–16], histological analyzes revealed no significant decreases in neuronal density near the implantation site compared to distant areas. Only mild elevation of astrocyte activation was observed within 30 μm of the uFINE-I, with no discernible accumulation of glial encapsulation surrounding the probe (Fig. 5e). In addition, the vascular injury caused by penetration healed with spindle cell hyperplasia following 30-day uFINE-I implantation, eliminating the risk of bleeding during chronic implantation (Fig. 5f). These results demonstrate the excellent biocompatibility and safety of uFINE-Is during chronic implantation, ensuring the potential for long-term usage in the future.

Viability in human clinical settings

To further explore the potential of uFINE-Is for future human clinical applications, we tested the same intravascular implantation system using a silicon model (32 cm × 17 cm × 20 cm, including the subclavian vein and part of the superior vena cava, Figs. 6a–d). This silicone model replicated the actual vessel lumen size of the brain venous system, based on measurements from an adult human male. The implantation device exhibited excellent navigability in this model. We achieved a seamless insertion process, smoothly advancing the device from the internal jugular vein to the SiS and then to the TrS for implantation in the visual cortex. We successfully positioned the device at the confluence of sinuses and penetrated the vessel precisely at the desired location (Fig. 6a).

We further tested whether our device could be generalized to non-branching areas in intracranial veins (Figs. 6b–d). We performed demonstrations to target the motor cortex (foot area near SSS and hand area near posterior frontal vein) and ventral striatum (near internal cerebral vein) due to their significant clinical relevance. The motor cortex serves as the primary target region for motor brain-machine interfaces[3,39], and the ventral striatum is the target of deep brain stimulation in treating refractory depression[40].To achieve directional puncture in non-branching areas, we leveraged the bending near the tip of the 4 F catheter to position the piercing device towards the target brain region at an ~45-degree angle relative to the vascular

axis. Additionally, a balloon catheter was employed to establish a support region to secure the puncture angle. Using this strategy, we successfully penetrated the vessel wall and delivered uFINE-Is to the areas corresponding to the motor cortex (foot and hand areas) and ventral striatum in the silicone model (Supplementary Movie 5). Therefore, our device and implantation procedure hold the potential to target multiple brain regions.

Moreover, we investigated the capability of uFINE-Is to be endothelialized within veins for future long-term implantation, as failure of endothelialization will constantly activate immune response due to the foreign body reaction. To test this, uFINE-Is were placed in the femoral veins of rats chronically. A thin layer of cells attached to the uFINE-I around 28 days post implantation[31] and as time progressed, we observed evident attachment of layers of endothelial cells on the surface of uFINE-Is at 3 months post-implantation (Fig. 6e). This endothelialization process is consistent with previous reports[41,42], which usually takes 3 months to develop and then stabilizes. In addition, no discernible signs of inflammation or necrosis, such as the enrichment of leukocytes, phagocytes, and eosinophils, appeared in the vessel walls and nearby tissues (Fig. 6e). Considering the small cross-sectional area of endothelialized uFINE-Is (0.0117 ± 0.0010 mm^2, mean ± SD, Fig. 6f, g), it will only occupy ~0.38% of the cross-sectional area in the human vein with a diameter of 2 mm, therefore should not significantly interfere with vessel patency. Taken together, it is evident that our unique intravascular implantation strategy for uFINE-Is holds immense promise for future clinical applications.

Discussion

We introduce an ultraflexible microelectrode capable of multi-channel single-unit recording in large animals with minimal invasiveness through an intravascular implantation strategy. To our knowledge, this is the first study that achieved direct implantation of electrodes into neural tissues in the brain via an intravascular approach involving navigation and penetration through blood vessels. Avoiding craniotomy fully preserves the benefits of the excellent biocompatibility of ultraflexible microelectrodes, which is critical to establishing stable neural interfaces. The evident endothelialization will also help secure uFINE-Is in place and facilitate the sealing between vessel walls and uFINE-Is during long-term implantation. Furthermore, we managed to overcome technical challenges and fabricate the uFINE-I at a length of 50 cm, which is ~12 times the length of typical ultraflexible microelectrodes[43] and ~6 times the length of published intravascular ultraflexible electrodes[31]. The extended length will enable the use of ultraflexible microelectrodes in future applications requiring long-distance spans. We also would like to bring up that the sheep venous structure is narrower, more tortuous, and highly branching than that in humans. The diameter of adult human venous vessels is approximately three to five times that of sheep vessels at comparable positions (e.g., sagittal sinus 4.3–9.9 mm v.s. 2–3 mm, great cerebral vein 4 mm v.s. 1.5 mm, transverse sinus 6.2–6.3 mm v.s. 2.5 mm, human v.s. sheep, see more detailed comparisons in Supplementary Table 3). Therefore, the
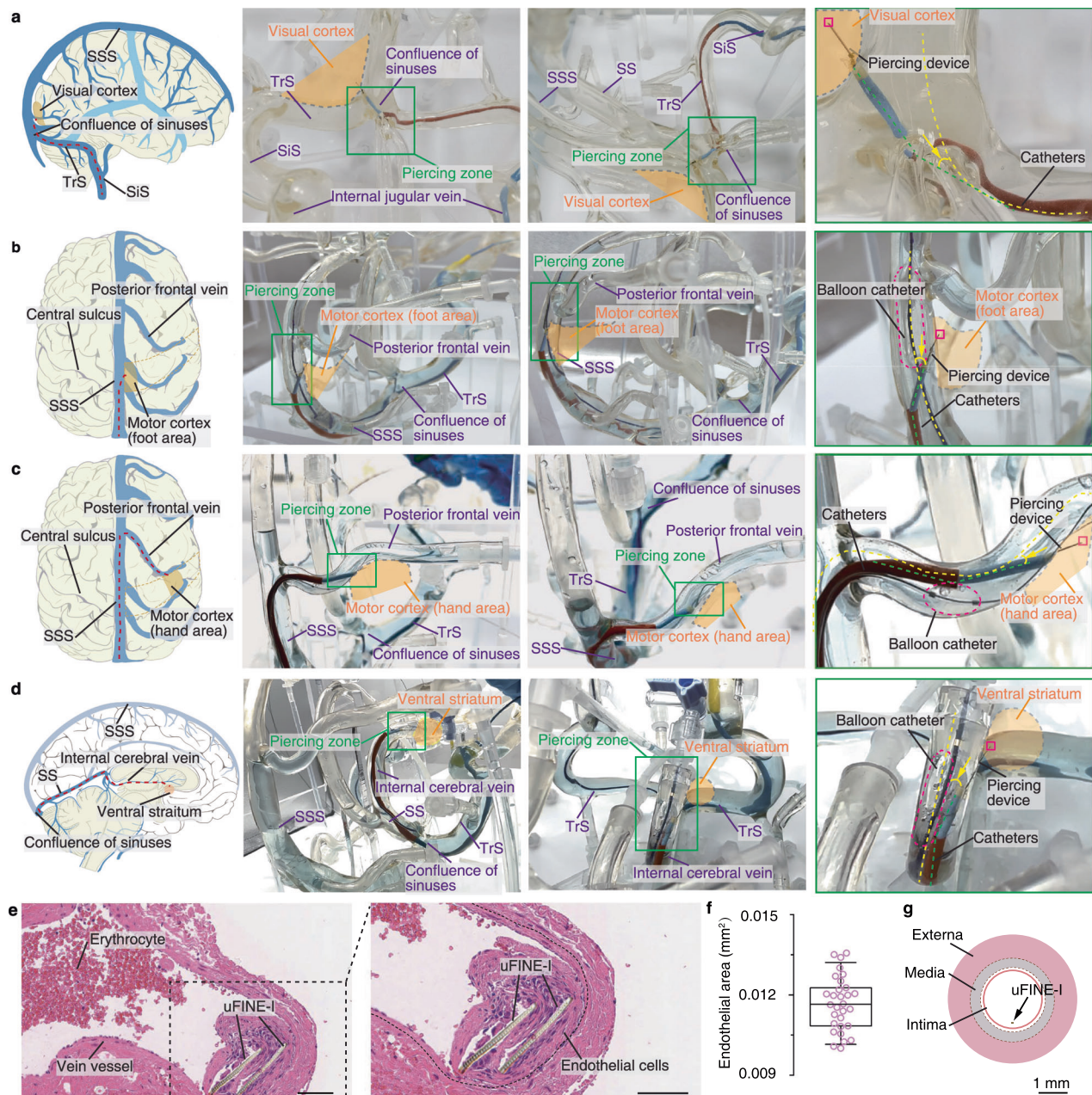
Fig. 6 | Viability in human clinical settings. a–d In vitro tests of the device navigability and electrode delivery in a human venous system model. The device smoothly reached the vascular areas near the visual cortex (**a**), the foot and hand area of the motor cortex (**b** and **c**), and the ventral striatum (**d**). The device penetrated the vessel wall at the desired location (indicated by green boxes) and delivered uFINE-Is to the target brain region (indicated by the orange shaded area). Red dashed lines in the leftmost column indicate intravascular paths. Magenta dashed lines outline balloon catheters. Yellow dashed lines indicate vascular axes. Green dashed lines indicate penetration directions. Yellow arrows indicate puncture angles. Magenta boxes indicate where the uFINE-I should be inserted in the target brain region. SS, straight sinus. Schematic diagrams were created based on ref. 64 **e** HE staining of the cross section of the femoral vein in rats, showing the endothelialization of uFINE-Is at 3 months after implantation. The black dashed line marks the intima in the magnified view. Scale bars, 100 and 50 μm. **f** The cross-sectional area of the endothelialized uFINE-I in the rat vein after 3-month implantation (0.0117 ± 0.0010 mm^2, $n = 30$ slices, mean ± SD). Boxed plot: the 25th, 50th (median), and 75th percentiles of the data are indicated. The whiskers represent mean ± 1.5 SD. **g** Schematic diagram showing the cross-sectional size of uFINE-I relative to human veins.

successful implantation in sheep strongly suggests that our intravascular strategy is readily expanded to clinical settings.

Compared with traditionally used rigid neural electrodes, uFINE-Is inherit the strengths of ultraflexible microelectrodes that the excellent biocompatibility ensures stable performance of neural interfaces in long-term implantation[14–16]. Although the uFINE-I could function as an endovascular electrode if combined with a stent structure as described in previous studies[31], we see that uFINE-Is and our intravascular implantation strategy outperform other neurointerventional electrodes from several aspects. First, the ultraflexibility and micron-scale dimensions enable the uFINE-I to fully utilize the vascular network and access more brain regions with distinct functions than other interventional electrodes. Reaching vessel branches close to the target brain region enables the collection of neural activity directly related to the function of interest, which is crucial to ensure the effectiveness of BMIs based on neural decoding. The piercing device we designed features an outer diameter of only 0.57 mm, minimizing the risk of damage to the brain and blood vessels.

Second, the uFINE-I is capable of recording single-unit activity in large animals at scale. Spiking activity is critical for enabling dexterous control of external devices (e.g., robotic arms)[44–46]. Although an endovascular ultraflexible electrode has successfully resolved the spiking activity of a few neurons in rats[31], our approach achieved a 2.3-fold increase in the single-unit yield. Meanwhile, it should be kept in mind that collecting spiking activity typically requires a neuron-electrode distance of less than 140 μm[47]. Successful spike detection in rats may be attributed to very thin walls of their vessels (10–20 μm in thickness). When transferred to larger animals or human patients, the ability to detect spikes may vary, influenced by the thickness of vessel walls, which can range from tens to 500 micrometers[48,49]. In contrast, the uFINE-I successfully recorded multi-channel spiking activity from the occipital lobe in a single sheep, readily be expanded to other large animal models and human patients. Furthermore, our implantation system leverages commercially mature catheter technology, which will facilitate its transition to future clinical applications.

Limitations

The prototype technology we present here is the first step that demonstrates the feasibility of multi-channel single-unit recording in large animals via intravascular strategies. A better recording performance can be achieved with improved electrode yield and optimized electrode configuration in future practical applications. Achieving single-unit recording in more experimental replicates covering various brain region targets and behavioral paradigms will further demonstrate the capability of the intravascular platform. To fit into the small space in the piercing device, the number of electrode sites was compromised to 30. The electron beam lithography will enable more compact layouts to accommodate more electrode sites, thereby increasing the recording density and scale of neural activity[50,51]. In addition, the current device can only implant one uFINE-I at a time, limiting the spatial coverage of neural recording and stimulation. Interventional devices that enable the implantation of multiple uFINE-I probes with minimized safety risk are required for sufficient spatial coverage in the future.

On the other hand, although uFINE-Is can detect single units in acute recordings, its long-term stability of neural recording needs further investigation. Long-term implantation in freely behaving animals would be ideal to test the functionality and translatability of our device, which requires integration with the wireless signal and power transmission systems. To allow the retraction of catheters from vascular pathways but leave the probe in place, the width of uFINE-I probes has to be < 2 mm. This presents significant technical challenges in the circumstance of intravascular delivery, as it requires a quick yet precise connection of 30 channels between the < 2-mm wide probe end and the wireless system. Furthermore, these procedures must be performed under sterile conditions in the surgical room. Developing a wireless system compatible with the uFINE-I and intravascular procedure will facilitate testing the functionality and translatability of our device in different application scenarios, such as motor neuroprosthetics and deep brain stimulation. Concurrently, a more comprehensive evaluation of behavioral deficits will be needed in future studies.

Although we have successfully demonstrated the feasibility of targeting the confluence of sinuses and nearby occipital lobe, the narrow and tortuous venous structure in sheep hindered our ability to target more brain regions effectively, forcing the use of a human silicone blood vessel model to assess the versatility of our device[52–59]. Interventional devices with smaller dimensions and better maneuverability are generally required to complete functionality tests in more brain regions in the animal model and reach more distal vascular branches in future clinical settings. Besides the brain regions demonstrated in this study, the potential sites include but are not limited to, the cingulate gyrus, hippocampus, amygdala, pineal gland, and hypothalamus. These brain regions are critical for supporting various aspects of daily life activities, from basic control of circadian rhythms and homeostasis to more complicated processing of emotion and decision-making. Delivery to these brain regions will be further explored to expand the applicable scenarios of our system to the investigation and treatment of a wide range of neurological diseases, such as sleep disorders and depression.

Leveraging the electrical stimulation capability of uFINE-Is is also one of our subsequent focuses. Many deep brain structures, such as the subthalamic nucleus and internal capsule, have become popular targets of neuromodulation in the treatment of neurological diseases[6]. We foresee that the electrode implantation in deep brain regions will greatly benefit from our intravascular strategy as accessing deeper brain regions via veins provides the most direct path, avoiding the damage caused by penetration through overlying brain structures in traditional SEEG or DBS surgical procedures. It may also reach brain structures that are critical to certain brain diseases but not targetable by traditional electrodes[60]. Correspondingly, the capability of uFINE-Is for neural stimulation remains to be demonstrated.

In conclusion, the uFINE-I and its intravascular implantation system together provide an innovative solution that enables single-unit recording and minimal invasiveness at the same time and can be readily expanded to clinical settings. We believe it will become a valuable tool applicable to a wide range of scenarios in both neuroscience research and clinical practice, advancing our understanding of the brain and improving the treatment of neurological diseases.

Methods

Design and fabrication of the ultraflexible implantable neural electrode for intravascular delivery (uFINE-I)

To adapt to the long delivery path in the intravascular implantation, the uFINE-I was designed as a single-shank electrode array, with a total length of 50 cm, a thickness of 5 μm, and an average width of 120 μm. Each uFINE-I contained 30 electrode sites at the tip for electrophysiological recording in vivo. Each site was in a circular shape with a diameter of 30 μm and the inter-electrode center distance was 40 μm.

The uFINE-I was fabricated using standard lithography (Supplementary Fig. 2) based on previously described procedures[16] with technical modifications. Polyimide (PI) was used as the base material as its high tensile strength ensured the integrity of uFINE-Is during navigation and penetration. To fit the 50-cm long uFINEs into the 6-inch silicon dioxide (SiO$_2$)-coated silicon (Si) wafer with a maximized radius of curvature, we placed uFINE-Is in a spiral configuration (Supplementary Fig. 2a). Detailed fabrication steps are as follows (Supplementary Fig. 2b).

i. The PI (U-Varnish S, UBE Corporation) was used to construct the insulating layers because of its excellent tensile strength, ease of fabrication, and chronic biostability[61,62]. The bottom insulating layer was spin-coated on the silicon (Si) wafer (300 nm thermal oxide, Szjxtech Co., Ltd) at 6000 rpm for 40 s, pre-baked sequentially at 65 °C for 10 min, 95 °C for 2 min, and 230 °C for 3 h.

ii. LOR 5 A (KAYAKU Advanced Materials, Inc.) was spin-coated at 2000 rpm for 35 s and baked at 180 °C for 3 min. Then AZ 5214 (Merck) was spin-coated at 2000 rpm for 45 s and baked at 95 °C for 2 min. The photoresist was patterned by photolithography with an ultraviolet optical musk aligner (SUSS MA6 mask aligner, SUSS MicroTec) and developed (AZ 300MIF, DuPont Electronic Materials) for 70 s. Following this photolithography process, a 50/800/200-nm-thick titanium/nickel/aurum (Ti/Ni/Au) bottom metal input/output (I/O) layer was deposited by E-beam evaporation (Ohmiker-60BL, Cello), followed by a lift-off step.

iii. The photolithography process for metal interconnects was similar to step ii. After that, 5/100/5-nm-thick Ti/Au/Ti was deposited by E-beam evaporation and lift-off.

iv. The coating and pre-baking processing in step i was repeated to define the top insulating layer.

v. AZ 5214 was spin-coated at 3000 rpm for 30 s and baked at 95 °C for 2 min, followed by photoresist patterning. The AZ 5214 was transferred to negative resist by baking at 120 °C for 40 s. Then, the wafer was exposed to an ultraviolet optical aligner without musk for 6 s, followed by a 60 s developing step. An 80-nm thick aluminum (Al) layer was deposited by E-beam evaporation and lift-off to protect PI of uFINE-I patterning under dry etching. The PI outside the Al protection layer was removed by reactive ion etching (SI591, Sentech) in 50% oxygen at 60 W for 110 min. Subsequently, the Al layer was etched by hydrofluoric acid (Titanium Etchant TFT, Transene) for 10 s, followed by adequate flush cleaning with deionized water.

vi. Following dry etching, hard baking was performed at 320 °C for 2 h. The extended curing time ensured sufficient strength while preserving flexibility for vascular navigation.

vii. The photolithography process in step ii was repeated to define 80 μm platinum (Pt) electrode regions for E-beam evaporation, followed by a lift-off step.

viii. Electrode site: The photolithography process in step ii was repeated to define 5/100-nm-thick Ti/Au electrode regions (30 μm in diameter) for E-beam evaporation. For those electrodes using IrO_x crystal to reduce impedance, the crystal was grown (PRO Line PVD 75, Kurt J. Lesker) at 130 W for 1200 s under argon and oxygen, followed by a lift-off step.

ix. The probe was released manually and carefully, and then attached to a specially trimmed little silicon chip slightly larger than the I/O section of uFINE-I by deionized water. After removing the water between the little silicon chip and the I/O section, the probe was soldered to a 128-channel FPC (flexible printed circuit) board of 42 mm in length, which was connected to the Intan headstage (Intan Technologies) for signal acquisition.

x. For electrode sites coated with PEDOT:PSS, PEDOT:PSS (Sigma-Aldrich Co.) was electrochemically coated on the gold contacts in an aqueous solution at a concentration of 43.04% w/v PEDOT and 0.13% w/v PSS. Constant current was applied to individual sites one by one using an Intan RHD electroplating board (Intan Technologies) at a current of 10 nA and 1-s cycle duration until the impedance at 1 kHz dropped below 100 kΩ[15].

Design and assembly of the intravascular piercing device

The assembly process for the device involved several steps to ensure proper alignment and functionality. Detailed process is as follows. We started with gathering all the necessary components of the device, including a microcatheter (Echelon, Medtronic) with customized length, a custom-made nickel-titanium microneedle, a custom-made nickel-titanium microwire, and 3D-printed handle parts. These components were cleaned thoroughly using alcohol and purified water to maintain sterility. First, the microneedle and microwire were assembled to ensure their coaxial alignment. As the microneedle and microwire should be able to protrude or retract independently, we adjusted their positions along the longest traveling dimension and fixed them using the 3D-printed parts (Formlabs). Next, the hole at the tip of the uFINE-I was hitched to the tip of microwire and the rest of the uFINE-I was straightened and coaxially aligned with the microneedle. The uFINE-I was housed and adjusted by the microwire to obtain the same tip placement with the microneedle. Finally, these semi-assembled units mentioned above were passed through the microcatheter until their tip positions were flush with each other. FPC was fixed on the assembly and all the parts were secured to ensure they remained in place.

In vitro characterization of the penetrating microneedle

The bending stiffness and puncture force of the nickel-titanium were measured to assess whether it was able to navigate in the tortuous veins safely and penetrate the vessel wall. To measure the bending stiffness and puncture force, the piercing device was securely fixed on a platform capable of moving forward at a constant speed. A force gauge (HP-2, Handpi) was also attached to the same platform. Before the test began, the 20-mm tip of the device was slightly attached to the tip of the force gauge which displayed a value of 0 at this point, and the axis was positioned perpendicular to the force direction (Fig. 2b, right). While the testing started, we pushed the device at a speed of ~2 mm/min, and then generated changes in force and bending angle within the device. As the device was being pushed forward, the entire testing process was recorded through video to capture the displacement, the deflection angle of the piercing device tip, as well as the force values exerted by the device. The force values were further analyzed in the Origin software (OriginLab). The bending angle of the piercing device was measured in the AutoCAD software (Autodesk) using image frames extracted from video recording. The puncture force measurement was conducted using a specialized apparatus (Shanghai Heng Instrument Factory Co. Ltd) to test the puncture force of medical injection needle tips, in accordance with the testing protocol prescribed in GB15811/ISO 7864 for Sterile Hypodermic Needles designed for single-use applications. Initially, the puncture needle was securely positioned in a vertical orientation within the testing instrument, with the needle diameter set to 0.3 mm to fulfill the test specifications. Subsequently, the apparatus was activated, causing the puncture needle to descend steadily at a rate of 1 mm/s, thereby piercing through a film material. The instrument recorded the variations in force exerted during the membrane penetration process. Upon the completion of the test, the puncture force was determined to be 1.654 ± 0.021 N (mean ± SD).

In vivo intravascular implantation surgery in sheep

Adult (70–75 kg) male sheep (Chinese Hu sheep, Beijing Longan Experimental Animal Breeding Center) were used for the study. All procedures were approved by the Institutional Animal Care and Use Committee Laboratory Animal Care Management Group. The surgical procedure was performed in a DSA (Canon Aquilion PRIME TSX-303A) catheterization room, and the entire procedure was strictly performed according to the protocol in clinical surgery. The skin of the animal was prepared before the operation. All direct contact consumables were sterilized with ethylene oxide.

Anesthesia and positioning: animals were housed individually and fasted from water and food for 12 h before surgery. Xylazine hydrochloride (Zhejiang Shengda Bio-Pharm Co., Ltd.) injection was used to induce anesthesia. The anesthetized sheep lay on the operating table in supine position, with the head tilted back and the trachea and mouth aligned to fully expose the epiglottis and glottis. An assistant held the laryngoscope to perform the endotracheal intubation procedure. The sheep was respiratorily anesthetized with isoflurane (3% for induction, 1.5% for maintenance, Matrix vaporizer) in a 30%/70% oxygen/nitrous oxide mixture.

Grounding wire connection: The sheep head was rotated to the right side, and a small incision of ~4 mm near the left parietal bone was made to expose the skull. A cranial screw was used as the grounding electrode. Then, the head was repositioned and soft cushions were used on both sides of the neck to secure the head in place.

Access preparation (Supplementary Figs. 3,4): We first located the middle and upper 1/3 junction of the sternoclavicular joint and the mastoid line, and performed a Seldinger technique puncture of the jugular vein, leaving a 6 F femoral artery sheath (RS*A60K10SQ, Terumo) in place. To adapt to the length of the sheep venous path, a 6 F guiding catheter (Tongbridge Medical) was trimmed to ~35 cm, and a 5 F guiding catheter (Chaperon, MicroVention) was trimmed to ~38 cm. These two guiding catheters were lined with each other and then advanced into the right transverse sinus (taking the right side as an example) under the guidance of a 0.035' hydrophilic guidewire

(Radifocus guidewire, Terumo). The 6 F and 5 F guiding catheters were further advanced to reach the middle or confluence of sinuses. If it was difficult to select the transverse sinus only using the guidewire, we would use a microcatheter (Prowler Select Plus, Medos International SARL, Le Locale, CH-2400) and a 0.014' microwire (Synchro 2, Stryker) to assist the selection. Finally, the 4 F inner catheter of the 5 F Chaperon catheter was replaced with a 4 F diagnostic catheter (INFINITI, Cordis) trimmed to ~38 cm, to provide better puncture support.

If the penetration direction, which was confined by the tip of the 4 F diagnostic catheter, was not satisfied, we would use the same method to perform a contralateral jugular vein penetration and sheath placement. In this case, both the 6 F and 5 F guiding catheters were advanced into the contralateral transverse sinus and then a 4.0 mm/7 mm balloon (Hyperform™ Occlusion Balloon System, Micro Therapeutics. Inc) was introduced via these two guiding catheters. By inflating the balloon at the confluence of sinuses, we were able to change the direction of the 4 F diagnostic catheter, which was placed in torcular Herophili via the contralateral transverse sinus, and finally adjusted the puncture direction.

Electrode penetration (Fig. 2 and Supplementary Fig. 4): The piercing device carrying the uFINE-I was inserted from the end of the retained 4 F diagnostic catheter until its tip exited the catheter tip. The interventionalist gently advanced the piercing device and stopped once feeling slight resistance. Then the piercing device was unlocked, and the puncture microneedle was advanced at a relatively fast speed by about 6 mm under the guidance of DSA. When the puncture microneedle departed from the venous sinus and entered the brain tissue, the interventionalist should feel a distinct breakthrough. Then the position of the puncture microneedle was further confirmed using C-arm CT (Canon Aquilion PRIME TSX-303A) to ensure it was out of the venous sinus. Further, the uFINE-I was advanced along the penetration direction by manually pushing the coupled microwire at the piercing device handle without any withdrawing. The advancing distance of the uFINE-I probe was determined based on the size of the target brain region and its location relative to the puncture site.

Signal acquisition: after the penetration was completed, the uFINE-I was connected to the data acquisition system. During this process, the depth of anesthesia as well as the depth of the puncture microneedle and the uFINE-I were adjusted to search for spikes.

Post-monitoring procedures: After data acquisition was completed, the uFINE-I and piercing device were withdrawn first, followed by the withdrawal of guiding catheters and 6 F artery sheath. When testing the feasibility of retaining the uFINE-I, the puncture microneedle was carefully retracted. Local pressure was applied at the incision site on the neck for 10 min to stop bleeding. The sheep was transported for a routine head CT scan to rule out intracranial bleeding. Then, the sheep was monitored until it resumed spontaneous breathing before the tracheal tube was removed. After that, the sheep was returned to the animal housing area.

Postoperative graded care was provided, incisions were disinfected daily, and the animal's condition was observed and recorded. Ceftriaxone sodium (Roche) was used intramuscularly for three days after the operation, and creatine phosphate sodium (Kaifeng Mingren Pharmaceutical) injection and glutathione (YAOPHARMA) injection were used according to the animal's condition. To ensure timely intervention and better prognosis, we also conducted a series of blood tests on the animals for a period spanning 3 to 7 days after the surgery, including five key parameters: blood routine test, blood biochemistry, blood gas, coagulation, and C-reactive protein (CRP).

Intravascular implantation surgery in rats

Four adult female rats (Sprague Dawley, 7-week old, Shanghai SLAC) were used in the study. All procedures were approved by the Institutional Animal Care and Use Committee Laboratory Animal Care Management Group. To examine the endothelialization of uFINE-Is, uFINE-

Is were implanted in the femoral veins in rats. The rats were under respiratory anesthesia with isoflurane throughout the implantation surgery. We started by fully disinfecting the rat legs using iodine. An incision in the skin tissue was made to expose the superficial femoral vein, which is attached to the thigh muscle group. Usually, a straight vein segment of ~7 mm in length was chosen as the target location for implantation. Then the injection needle (32 G), which carried the uFINE-I, gently punctured the target blood vessel wall and advanced 5 mm forward in the lumen. During this process, we carefully avoided puncturing other locations in the vein to maintain the vessel's integrity. Once the uFINE-I was in place, the injection needle was carefully withdrawn and pressure was immediately applied to puncture sites to stop any bleeding. We usually implanted one or two uFINE-Is in a single segment of the femoral vein. After the surgical procedure, rats were placed back into their home cages for recovery. The uFINE-Is were left in rats for 3 months. After that, the rats were anesthetized with isoflurane. Both ends of the target blood vessel were ligated or securely tied, effectively isolating the segment where the uFINE-Is were implanted. Then the central portion of the blood vessel containing uFINE-Is was extracted for further histological analysis. Extracted tissue samples were meticulously fixed in a 4% paraformaldehyde (PFA) solution. Following fixation, the tissue sample was sliced at a thickness of 5 μm and subject to the standard Hematoxylin and Eosin (HE) staining procedure (Fig. 6e). The cross-sectional area of endothelialized uFINE-Is was quantified using the Fiji software (ImageJ).

Electrophysiological recording and analysis

The uFINE-I was connected to an Intan 128-channel recording headstage (Intan Technologies) via FPC and a custom-made connector board. Raw signals were recorded at 30 kHz using the Intan RHD2000 system (Intan Technologies), along with impedance measurements. Synchronization between visual stimuli and electrophysiological recording was achieved by TTL pulses.

The LFPs and vascular ECoG signals were lowpass filtered (< 500 Hz, 4th-order Butterworth filter) in both forward and reverse directions to prevent phase distortion (Figs. 3b, 4b, c). Spike sorting was performed with OfflineSorter (V2, Plexon). Before sorting, the mean value from each channel was subtracted and the common average referencing was removed by median across channels. Here we sorted single units based on the principal component distributions, waveforms, and inter-spike intervals as features. Spike waveforms were clustered using the k-means algorithm. We conservatively retained units that were distinct from noise and from each other. Units that had more than 2% of their post-sorted spikes within the refractory period (2 ms) were classified as multi-units and discarded from the analysis. The signal-to-noise ratio was calculated as the peak-to-trough amplitude of the mean waveform divided by twice the standard deviation of the remaining data stream after all waveforms were removed (Fig. 3c).

To classify single units that were responsive or nonresponsive to visual stimuli (Fig. 3b, right), the mean firing rate during 500 ms before and after the visual stimulation event (light onset or offset) in each trial was quantified for Wilcoxon signed rank test. Significance was defined by an alpha pre-set to 0.05.

Postoperative safety assessment

For the purpose of histological analysis, sheep were sacrificed at specific time points, including on the day of surgery, as well as at 7 and 30 days postoperatively. Ensuring the proper fixation of the sheep brain tissue was a critical step of this process. As sheep are much larger than rodents, we adopted a perfusion method specifically designed for sheep[63]. We initially administered respiratory anesthesia to the sheep while it was still alive. Subsequently, the sheep's neck was sterilized, and the skin in this region was carefully prepared for the upcoming steps. The carotid arteries and jugular veins located on both sides of the sheep's neck were exposed for accessibility. A silicon tube (~5 mm

in diameter) with two branches was first filled with saline and then its two branches were inserted into the carotid arteries on both sides of the sheep's neck. The other end of this silicon tube was connected to a peristaltic pump (ELP02-D12, Kamoer). Another silicon tube with two branches was used to connect the bilateral jugular veins to a suction device. This system was essential for the controlled distribution of the saline and formalin solution. Once the entire perfusion system was secured in place, the pump was activated. Saline was first pumped into vessels to flush blood away. Then the formalin solution was pumped in and distributed throughout the cranial region. Stiffening of body mussels indicated the successful fixation of the brain tissue. The brain and main internal organs (heart, liver, spleen, lung, and kidney) were collected and fixed in 4% PFA.

Following the tissue fixation process, three-μm thick sagittal sections of the sheep brain were sliced by a microtone. For the histological analyzes of acute uFINE-I implantation (Fig. 5d), sections were blocked in a bovine serum albumin solution for 30 min at room temperature and then incubated overnight at 4 °C with primary antibodies (1:200 rabbit anti-glial fibrillary acidic protein (GFAP), Servicebio). A washing procedure was meticulously carried out and the sections were incubated with Alexa Flour-conjugated secondary antibodies (1:200 anti-rabbit 488, Servicebio) for 50 min at room temperature. For the histological analyzes of chronic uFINE-I implantation (Fig. 5e), multiplex immunohistochemistry was performed for histological analyzes (primary antibodies: 1:200 rabbit anti-GFAP, abcam; 1:3000 rabbit anti-NeuN, abcam; secondary antibodies: anti-rabbit 488, Dako; anti-rabbit 520, Dako). Then sections were mounted using a mounting medium for DAPI (4',6-diamidino-2-phenylindole) staining, and imaged using a fluorescence scanner (Pannoramic MIDI, 3DHISTECH).

For chronic uFINE-I implantation experiments, to help locate the site of electrode puncture into the brain, we coated the tip of the piercing device with a fluorescent dye (CellTracker CM-DiI, C7000, Thermo Fisher) before implantation. This fluorescent dye was carried to the brain surface by the piercing device and retained in living cells for 30 days. During the dissection at 30 days post-implantation, we first identified the puncture site based on the fluorescence on the brain surface under a fluorescence microscope (ApoTome.2, Zeiss), and subsequently conducted histological analyzes on the brain tissue around the puncture site. The implantation trajectory was meticulously identified by footprints that resembled the cross-sectional size of uFINE-I and spanned continuous brain slices.

In-vitro test on the human intracranial venous system model

To evaluate the performance of the piercing device and catheter system in reaching multiple brain areas, we used a custom-made silicone model of the human intracranial venous system. The piecing device, guidewires, and catheters test in this silicon model were same as those used in sheep experiments. To reach the visual cortex, we built catheter access through the pathway of SiS-TrS-confluence of sinuses. To reach the foot area of the motor cortex, we built catheter access through the pathway of SiS-TrS-confluence of sinuses-SSS. To reach the hand area of the motor cortex, we built catheter access through the pathway of SiS-TrS-confluence of sinuses-SSS-posterior frontal vein. To reach the ventral striatum, we built catheter access through the pathway of SiS-TrS-confluence of sinuses-SS-internal cerebral vein. Besides the visual cortex, other target brain regions were near non-branching veins and penetration in these vascular areas necessitated a balloon catheter to provide extra puncture support. To achieve directional puncture in the non-branching area, we leveraged the bending close to the tip of the 4 F catheter, which together with the balloon catheter positioned the piercing device towards the target brain region at a 45-degree angle relative to the vascular axis. The critical steps of in vitro test in non-branching veins are described below:

i. **Navigation:** Use a guidewire to navigate the guiding catheters to the vascular zone near the target brain area. The 0.035' guidewire was selected and advanced along with 6 F guiding catheter. Then retrieve the guidewire.

ii. **Establishing Catheter Pathway:** Deliver the 4 F catheter through guiding catheter to the target vascular zone for penetration (piercing zone). Adjust the direction of the catheter tip and establish a pathway for the piercing device.

iii. **Balloon Delivery:** Deliver the balloon catheter along with guidewire to reach the vessel position slightly distal to the piercing zone (e.g., the foot area of the motor cortex) or just in the piercing zone (e.g., the hand area of the motor cortex). Engorge the balloon to establish puncture support.

iv. **Position Evaluation:** Within the piercing zone, evaluate the position of the balloon and 4 F catheter tip. The position of each can be specifically adjusted in the piercing zone. The goal is to form an acute angle relative to the vessel wall for the access of puncture microneedle, making it point towards the target brain area.

v. **Penetration and uFINE-I Implantation:** Perform the vessel penetration and further advance the uFINE-I via guiding microwire.

Statistics and reproducibility

No statistical methods were used to predetermine sample sizes, but our sample sizes are similar to those reported in previous publications in the field. No randomization was performed. Randomization is not necessary to our study because all animals underwent the same surgical and recording procedures. Data collection and analysis were not performed blind to the conditions of the experiments.

Reporting summary

Further information on research design is available in the Nature Portfolio Reporting Summary linked to this article.

Data availability

All data supporting the findings of this study are available within the article and its supplementary files. Any additional requests for information can be directed to, and will be fulfilled by, the corresponding authors. Source data are provided with this paper.

References

1. Rezeika, A. et al. Brain–computer interface spellers: A review. *Brain Sci.* **8**, 57 (2018).
2. Kawala-Sterniuk, A. et al. Summary of over fifty years with brain-computer interfaces—a review. **11**, 43 (2021).
3. Hochberg, L. R. et al. Reach and grasp by people with tetraplegia using a neurally controlled robotic arm. *Nature* **485**, 372–375 (2012).
4. Collinger, J. L. et al. High-performance neuroprosthetic control by an individual with tetraplegia. *Lancet* **381**, 557–564 (2013).
5. Flesher, S. N. et al. A brain-computer interface that evokes tactile sensations improves robotic arm control. **372**, 831–836 (2021).
6. Lozano, A. M. et al. Deep brain stimulation: current challenges and future directions. *Nat. Rev. Neurol.* **15**, 148–160 (2019).
7. Sui, Y. et al. Deep brain–machine interfaces: sensing and modulating the human deep brain. *Natl. Sci. Rev.* **9**, nwac212 (2022).
8. Morrell, M. J. Responsive cortical stimulation for the treatment of medically intractable partial epilepsy. **77**, 1295–1304 (2011).
9. Cook, M. J. et al. Prediction of seizure likelihood with a long-term, implanted seizure advisory system in patients with drug-resistant epilepsy: a first-in-man study. *Lancet Neurol.* **12**, 563–571 (2013).
10. Steinmetz, N. A. et al. Neuropixels 2.0: a miniaturized high-density probe for stable, long-term brain recordings. **372**, eabf4588 (2021).
11. Dutta, B. et al. in 2019 IEEE International Electron Devices Meeting (IEDM) 10.11.11-10.11.14 (2019).

12. Kozai, T. D. Y., Jaquins-Gerstl, A. S., Vazquez, A. L., Michael, A. C. & Cui, X. T. Brain tissue responses to neural implants impact signal sensitivity and intervention strategies. *ACS Chem. Neurosci.* **6**, 48–67 (2015).

13. Barrese, J. C., Aceros, J. & Donoghue, J. P. Scanning electron microscopy of chronically implanted intracortical microelectrode arrays in non-human primates. *J. Neural Eng.* **13**, 026003 (2016).

14. Luan, L. et al. Ultraflexible nanoelectronic probes form reliable, glial scar–free neural integration. **3**, e1601966 (2017).

15. Zhao, Z. et al. Ultraflexible electrode arrays for months-long high-density electrophysiological mapping of thousands of neurons in rodents. *Nat. Biomed. Eng.* **7**, 520–532 (2023).

16. Tian, Y. et al. An ultraflexible electrode array for large-scale chronic recording in the nonhuman primate brain. *Adv Sci (Weinh)* **10**, e2302333 (2023).

17. Lycke, R. et al. Low-threshold, high-resolution, chronically stable intracortical microstimulation by ultraflexible electrodes. *Cell Rep.* **42**, 112554 (2023).

18. Campbell, A. & Wu, C. J. M. Chronically implanted intracranial electrodes: tissue reaction and electrical changes. **9**, 430 (2018).

19. Eles, J., Vazquez, A., Kozai, T. & Cui, X. J. B. Meningeal inflammatory response and fibrous tissue remodeling around intracortical implants: an in vivo two-photon imaging study. **195**, 111–123 (2019).

20. McConnell, G. C. (2008) https://core.ac.uk/download/pdf/4719864.pdf.

21. Forbes, Thomas et al. Comparison of surgical, stent, and balloon angioplasty treatment of native coarctation of the aorta. *J. Am. Coll. Cardiol.* **58**, 2664–2674 (2011).

22. Kolte, D. et al. Endovascular versus surgical revascularization for acute limb ischemia. **13**, e008150 (2020).

23. Murray, T. É. et al. Treatment of visceral artery aneurysms using novel neurointerventional devices and techniques. *J. Vasc. Interventional Radiol.* **30**, 1407–1417 (2019).

24. Loftus, C. M., Hoffmann, M., Heetderks, W., Zheng, X. & Peña, C. Regulation of neurological devices and neurointerventional endovascular approaches for acute ischemic stroke. **9**, 320(2018).

25. Crinnion, W. et al. Robotics in neurointerventional surgery: a systematic review of the literature. **14**, 539–545 (2022).

26. Loh, S.X. et al. Coils embolization use for coronary procedures: Basics, indications, and techniques. *Catheter Cardiovasc Interv.* **102**, 900–911 (2023).

27. Kang, D.-H. et al. Direct thrombus retrieval using the reperfusion catheter of the penumbra system: forced-suction thrombectomy in acute ischemic stroke. **32**, 283–287 (2011).

28. Frei, D. et al. The SPEED study: initial clinical evaluation of the Penumbra novel 054 reperfusion catheter. **5**, i74-i76 (2013).

29. Mitchell, P. et al. Assessment of safety of a fully implanted endovascular brain-computer interface for severe paralysis in 4 patients: the stentrode with thought-controlled digital switch (SWITCH) study. **80**, 270–278 (2023).

30. Thielen, B. et al. Making a case for endovascular approaches for neural recording and stimulation. **20**, 011001 (2023).

31. Zhang, A. et al. Ultraflexible endovascular probes for brain recording through micrometer-scale vasculature. **381**, 306–312 (2023).

32. Lylyk, P. et al. First-in-human endovascular treatment of hydrocephalus with a miniature biomimetic transdural shunt. **14**, 495–499 (2022).

33. Yaeger, K. & Mocco, J. J. N. C. *Future directions Endovasc. Neurosurg.* **33**, 233–239 (2022).

34. Oxley, T. J. et al. An ovine model of cerebral catheter venography for implantation of an endovascular neural interface. *J. J. Neurosurg. Jns.* **128**, 1020–1027 (2018).

35. John, S. E. et al. Vascular remodeling in sheep implanted with endovascular neural interface. *J. Neural Eng.* **19**, 056043 (2022).

36. Clarke, P. & Whitteridge, D. The cortical visual areas of the sheep. *J. Physiol.* **256**, 497–508 (1976).

37. Mazade, R. et al. Cortical mechanisms of visual brightness. *Cell Rep.* **40**, 111438 (2022).

38. Kinoshita, M. & Komatsu, H. Neural representation of the luminance and brightness of a uniform surface in the macaque primary visual cortex. *J. Neurophysiol.* **86**, 2559–2570 (2001).

39. Pandarinath, C. et al. High performance communication by people with paralysis using an intracortical brain-computer interface. *elife* **6**, e18554 (2017).

40. Malone, D. A. Jr et al. Deep brain stimulation of the ventral capsule/ventral striatum for treatment-resistant depression. *Biol. psychiatry* **65**, 267–275 (2009).

41. Jana, S. Endothelialization of cardiovascular devices. *Acta Biomaterialia* **99**, 53–71 (2019).

42. Marston, W. A., Chinubhai, A., Kao, S., Kalbaugh, C. & Kouri, A. In vivo evaluation of safety and performance of a nitinol venous stent in an ovine iliac venous model. *J. Vasc. Surg.: Venous Lymphatic Disord.* **4**, 73–79 (2016).

43. Seo, K. J. et al. A soft, high-density neuroelectronic array. *Npj Flex. Electron.* **7**, 40 (2023).

44. Hochberg, L. R. et al. Neuronal ensemble control of prosthetic devices by a human with tetraplegia. *Nature* **442**, 164–171 (2006).

45. George, J. A. et al. Long-term performance of Utah slanted electrode arrays and intramuscular electromyographic leads implanted chronically in human arm nerves and muscles. *J. Neural Eng.* **17**, 056042 (2020).

46. Wendelken, S. et al. Restoration of motor control and proprioceptive and cutaneous sensation in humans with prior upper-limb amputation via multiple Utah Slanted Electrode Arrays (USEAs) implanted in residual peripheral arm nerves. *J. Neuroeng. Rehabilitation* **14**, 121 (2017).

47. Buzsáki, G. Large-scale recording of neuronal ensembles. *Nat. Neurosci.* **7**, 446–451 (2004).

48. Müller, B. et al. in Developments in X-ray tomography VI, **7078**, 89–98 (SPIE, 2008).

49. Camasão, D. & Mantovani, D. The mechanical characterization of blood vessels and their substitutes in the continuous quest for physiological-relevant performances. a critical review. *Mater. Today Bio* **10**, 100106 (2021).

50. Scholvin, J. et al. Close-packed silicon microelectrodes for scalable spatially oversampled neural recording. *IEEE Trans. Biomed. Eng.* **63**, 120–130 (2016).

51. Wei, X. et al. Nanofabricated ultraflexible electrode arrays for high-density intracortical recording. **5**, 1700625 (2018).

52. Hoffmann, A. et al. The ovine cerebral venous system: comparative anatomy, visualization, and implications for translational research. *PLoS One* **9**, e92990 (2014).

53. HAZIROĞLU, M. Gross anatomy of dural sinuses in sheep. *Ank. Üniversitesi Vet. Fak. ültesi Derg.* **41**, 533–539 (1994).

54. Andrews, B. T., Dujovny, M., Mirchandani, H. G. & Ausman, J. I. Microsurgical anatomy of the venous drainage into the superior sagittal sinus. *Neurosurgery* **24**, 514–520 (1989).

55. Kong, Q., Sacca, V., Zhu, M., Ursitti, A. K. & Kong, J. Anatomical and functional connectivity of critical deep brain structures and their potential clinical application in brain stimulation. *J. Clin. Med.* **12**, 4426 (2023).

56. Tubbs, R. S., Loukas, M., Shoja, M. M., Bellew, M. P. & Cohen-Gadol, A. A. Surface landmarks for the junction between the transverse and sigmoid sinuses: application of the "strategic" burr hole for suboccipital craniotomy. *Operative Neurosurg.* **65**, ons37–ons41 (2009).

57. Altafulla, J. J., Prickett, J., Iwanaga, J., Dumont, A. S. & Tubbs, R. S. Intraluminal anatomy of the transverse sinus: implications for endovascular therapy. *Anat. Cell Biol.* **53**, 393 (2020).

58. Backes, W. H. & Nijenhuis, R. J. *Mapping the Vasculature of the Spinal Cord*, *Quantitative MRI of the Spinal Cord*, Academic Press, 258–264 (2014).

59. Khan, Y. S. & Lui, F. *Neuroanatomy, Spinal Cord*. In: StatPearls. StatPearls Publishing, Treasure Island (FL), (2020).

60. Neudorfer, C. et al. Endovascular deep brain stimulation: investigating the relationship between vascular structures and deep brain stimulation targets. *Brain Stimulation* **13**, 1668–1677 (2020).

61. Schander, A., Gancz, J. M., Tintelott, M. & Lang, W. Towards long-term stable polyimide-based flexible electrical insulation for chronically implanted neural electrodes. *Micromachines* **12**, 1279 (2021).

62. Vomero, M. et al. On the longevity of flexible neural interfaces: establishing biostability of polyimide-based intracortical implants. *Biomaterials* **281**, 121372 (2022).

63. Santoreneos, S., Stoodley, M. A., Jones, N. R. & Brown, C. J. A technique for in vivo vascular perfusion fixation of the sheep central nervous system. *J. Neurosci. methods* **79**, 195–199 (1998).

64. Rhoton Jr, A. L. et al. *Rhoton's Cranial Anatomy And Surgical Approaches*. (Oxford University Press, 2019).

Acknowledgements

Author contributions

Conceptualization: X.W., Z.Z., Methodology: X.W., Z.Y., S.W., H.Y., C.G., Z.Z., Y.B., C.R., X.L., Investigation: X.W., Z.Y., S.W., H.Y., C.G., Z.Z., C.R., Y.B., Y.D., J.C., Z.L., Y.W., Visualization: X.W., Z.Y., S.W., C.R., Y.B., Funding acquisition: Z.Z., X.L., Project administration: X.W., Z.Z., Supervision: Z.Z., C.R., Writing – original draft: X.W., C.R., Z.Y., S.W., Writing – review & editing: X.W., C.R., Z.Z., Z.Y.

Competing interests

Z.Z., X.L., and X.W. are co-inventors on a patent filed by CAS Center for Excellence in Brian Science and Intelligence Technology (CN202210697115.5, 2022) on the intravascular implantation system related to this study. The other authors declare no competing interest.

Additional information

Supplementary information The online version contains supplementary material available at https://doi.org/10.1038/s41467-024-53720-5.

Correspondence and requests for materials should be addressed to Chi Ren, Zhigang Yang or Zhengtuo Zhao.

Peer review information *Nature Communications* thanks the anonymous reviewers for their contribution to the peer review of this work. A peer review file is available.

Reprints and permissions information is available at http://www.nature.com/reprints

Publisher's note Springer Nature remains neutral with regard to jurisdictional claims in published maps and institutional affiliations.